J.Korean Asso. Radiat. Prot.
Vol.26 No.3 : 167-175(2001)

▣Papers▣

THIN-FILM-COATED DETECTORS FOR NEUTRON DETECTION

Douglas S. McGregor, Holly K. Gersch, Jeffrey D. Sanders
SMART Laboratory, NERS, 2600 Draper, University of Michigan, Ann Arbor, MI 48109-2145

Raymond T. Klann
Argonne National Laboratory, 9700 S. Cass Ave., Argonne, IL 60439

John T. Lindsay
Phoenix Memorial Laboratory, University of Michigan, Ann Arbor, MI 48109-2100

Abstract - Semiconductor diode detectors coated with neutron reactive material are presently under investigation for various uses, such as remote sensing of thermal neutrons, fast neutron counting, and thermal neutron radiography. Theory indicates that single-coated devices can yield thermal neutron efficiencies from 4% to 11%, which is supported by experimental evidence. Radiation endurance measurements indicate that the devices function well up to a limiting thermal neutron fluence of $10^{13}/cm^2$, beyond which noticeable degradation occurs. Thermal neutron contrast images of step wedges and simple phantoms, taken with dual in-line pixel devices, show promise for thermal neutron imaging detectors.

INTRODUCTION

Semiconductors coated with neutron reactive marterials, such as ^{10}B, ^{6}LiF, Gd, or plastics offer a method of realizing compact and rugged detectors for thermal and fast neutrons [1-17]. The entire device, including the package, can be less than a mm thick while allowing for thermal neutron efficiencies of 4% or greater, depending upon the configuration. Several semiconductors have been tried as detector substrates for thin-film coated neutron detectors including Si, SiC, amorphous Si, diamond and GaAs [1-17]. In the present work, GaAs is under investigation because of the relative fabrication ease by which devices can be manufactured, their relatively good radiation hardness, and their operational simplicity [3-6, 18].

Thin-film neutron detectors can be used in a variety of scenarios, including real time personal dose monitoring (as allowed by "self-biased" devices), neutron radiography (as allowed by high density neutron imaging arrays), directional fast neutron detection (as allowed by polyethylene-coated devices), and compact remote monitors in hostile radiation environments.

THEORETICAL CONSIDERATIONS

1. ^{10}B coatings

The microscopic thermal neutron absorption cross section (σ) for ^{10}B is 3840 barns, which is a relatively high value and is one of the main reasons why ^{10}B is used for thermal neutron detection. The microscopic neutron absorption cross section decreases with increasing neutron energy, with a dependence proportional to the inverse of the neutron velocity ($1/\nu$) over much of the energy range [19]. The atomic density for pure

^{10}B is 1.3 × 10^{23} atoms/cm^3, resulting in a macroscopic thermal neutron absorption cross section (Σ) of 500/cm. The $^{10}B(n,\alpha)^7Li$ reaction leads to the following products [20]:

$$^{10}B + {}^1_0n \rightarrow \begin{cases} {}^7Li\,(at\,1.015\,MeV) + \alpha\,(at\,1.777\,MeV), & 2.792\ MeV\,(to\ ground\ state) \\ {}^7Li^*\,(at\,0.840\,MeV) + \alpha\,(at\,1.470\,MeV), & 2.310\ MeV\,(1st\ excited\ state) \end{cases}$$

Reaction Q- Value

which are released in opposite directions when thermal neutrons (0.0259 eV) are absorbed by ^{10}B. After absorption, 94% of the reactions leave the ^7Li ion in its first excited state, which rapidly de-excites to the ground state ($\sim 10^{-13}$ seconds) by releasing a 480 keV γ-ray. The remaining 6% of the reactions result in the ^7Li ion dropping directly to its ground state.

Either an α-particle or a ^7Li ion reaction product may reach the detector after a $^{10}B(n,\alpha)^7Li$ reaction. If so, the energy registered by the detector is simply the original particle energy minus the energy absorbed in the boron film and detector contact during transit. The device contacts are very thin, and it can be assumed that energy loss in the detector contact is negligible. At any reaction location within the ^{10}B film, the maximum detector entrance energy will be retained by either particle should it enter the detector in an orthogonal trajectory. For the same interaction distance from the detector, the energy retained by the particle when it reaches the detector decreases as the angle exceeds orthogonality.

The average range for a 0.840 MeV ^7Li ion in pure ^{10}B is 1.6 μm and the average range for a 1.47 MeV α-particle in pure ^{10}B is 3.6 μm. At the end of the average range, the charged particle no longer has any energy and can not be detected. The longest range that a particle can transit through the reactive film and still retain detectable energy for a given system is referred to as the effective range, L. Given a predetermined lower level discriminator (LLD) setting, the average effective range (L) for either particle can be determined. For example, an LLD setting of 300 keV yields a calculated value of L_{Li} = 0.810 μm for 840 keV ^7Li ions and L_α = 2.648 μm for 1.47 MeV α-particles. At 300 keV, the ΣL product for 840 keV ^7Li ions is 0.0405, and the ΣL product for 1.47 MeV α-particles is 0.1324.

2. ^6Li coatings

Pure ^6Li can be used as a neutron reactive coating, although its corrosive and reactive nature results in cumbersome handling procedures. The $^6Li(n,\alpha)^3H$ reaction leads to the following products:

$$^6Li + {}^1_0n \rightarrow {}^3H\,(at\,2.73\,MeV) + \alpha\,(at\,2.05\,MeV), \qquad 4.78\ MeV$$

Reaction Q- Value

which are oppositely directed if the neutron energy is sufficiently small. Although the thermal neutron absorption cross section for ^6Li is lower than with ^{10}B, the higher reaction product energies make it attractive for thermal neutron detection. The microscopic thermal neutron (0.0259 eV) absorption cross section for pure ^6Li is 940 barns. The microscopic neutron absorption cross section also demonstrates a 1/v dependence. Pure ^6Li has a mass density of 0.463 g/cm^3 and an atomic density of 4.634 x 10^{22} atoms/cm^3. The macroscopic thermal neutron absorption cross section is 43.56/cm.

The low atomic density and the low mass density of pure ^6Li result in rather large reaction product ranges [6]. With an *LLD* setting of 300 keV, the values of L for the pure ^6Li film far surpass those calculated for the pure ^{10}B film, with $L\alpha$ = 19.05 μm and L_H = 126.77 μm. Hence, thick reaction product films must be deposited to achieve optimum performance, which can be difficult to deposit and prevent from decomposing.

A popular stable compound of ^6Li used for neutron detection is ^6LiF. The atom density of ^6LiF is 6.118 x 10^{22} /cm^3 and the mass density is 2.541 g/cm^3. With a microscopic thermal neutron cross section of 940 barns for ^6Li, the resulting macroscopic thermal neutron cross section for ^6LiF is 57.51/cm. An *LLD* setting of 300 keV gives $L\alpha$ as 4.64 μm and L_H as 29.25 μm [6]. At 300 keV, the ΣL product for 2.05 MeV α-particles is 0.0267 and the ΣL product for 2.73 MeV tritons is 0.1682. The ΣL

products for ^{6}LiF are very similar to than those of pure ^{10}B, indicating that their maximum achievable thermal neutron efficiencies should also be similar.

3. Theoretical Efficiency

It can be shown that the neutron detection efficiency is [3,6]:

$$S_p(D_F) = 0.5F_p\left\{\left(1+\frac{1}{\Sigma_F L}\right)\left(1-e^{-\Sigma_F D_F}\right)-\frac{D_F}{L}\right\},$$

for , $D_F \le L$, (1)

and

$$S_p(D_F) = 0.5\,F_p\,e^{-\Sigma_F (D_F - L)}\left\{\left(1+\frac{1}{\Sigma_F L}\right)\left(1-e^{-\Sigma_F L}\right)-1\right\},$$

for , $D_F > L$, (2)

where DF is the reactive film thickness and Fp refers to the branching ratio of the reaction product emission. The total efficiency can be found by summing each of the reaction product efficiencies:

$$S(D_F)\big|_{Total} = \sum_{p=1}^{N} S_p(D_F) \quad , \tag{3}$$

where N is the number of possible reaction product emissions at different energies. In the case of ^{10}B-based films, N equals 4 whereas for ^{6}Li-based films, N equals 2. Notice from Equation 2 that the value of S_p decreases as D_F exceeds the value of L. Films thicker than L for the long-range reaction product serve to only absorb neutrons without increasing the detection efficiency. The efficiency decreases with increasing film thickness because neutrons are absorbed in the outermost film layer without the charged-particle reaction products reaching the detector. The maximum range of the charged particles in addition to the neutron cross section will set an absolute limit on the intrinsic efficiency of the detector. As a result, there will be an optimal neutron reactive film thickness for frontally irradiated detectors. The optimal film thickness is also a function of the *LLD* setting [3].

For backside irradiation, the effect of the substrate upon the neutron beam must be accounted for. It is best to use semiconductor substrates with low thermal neutron interaction cross sections, such as Si or SiC. The neutron intensity reaching the reactive film can be represented by

$$I\big|_{\text{interface}} = I_0 \prod_{i=1}^{M} e^{-\Sigma_i D_i} \quad , \tag{4}$$

where I_0 is the initial neutron beam intensity, Σ_i is the macroscopic cross section for each layer, D_i is the thickness of each layer, and M is the number of detector layers excluding the thermal neutron reactive film. Assuming orthogonal backside irradiation, the sensitivity can be shown to be

$$S_p(D_F) = 0.5F_p \prod_{i=1}^{M} e^{-\Sigma_i D_i}\left\{\left(1-\frac{1}{\Sigma_F L}\right)\left(1-e^{-\Sigma_F D_F}\right)+\frac{D_F}{L}e^{-\Sigma_F D_F}\right\} \quad , \quad D_F \le L \quad , \tag{5}$$

and

$$S_p(D_F) = 0.5\,F_p \prod_{i=1}^{M} e^{-\Sigma_i D_i}\left\{\left(1-\frac{1}{\Sigma_F L}\right)\left(1-e^{-\Sigma_F L}\right)+e^{-\Sigma_F L}\right\} \quad , \quad D_F > L \quad . \tag{6}$$

Contrary to the front irradiation case, the lowest neutron interaction rate within the reactive film is the farthest distance from the film-detector junction, and the highest neutron interaction rate within the reactive film is adjacent to the film-detector junction. As a result, the backside irradiated devices can achieve slightly higher neutron sensitivities than front side irradiated devices.

Using *LLD* settings of 300 keV, Figures 1 and 2 show the expected thermal neutron detection efficiency for ^{10}B, ^{6}LiF, and pure ^{6}Li films as a function of film thickness. In all cases, backside irradiation allows for slightly higher efficiency than front side irradiation. Figure 1 shows that only a slight efficiency increase is achieved by using ^{6}LiF (4.3%) instead of ^{10}B (4%), yet the ^{6}LiF film thickness required to match the efficiency of ^{10}B is almost 8 times greater. Figure 2 shows the expected efficiency for pure ^{6}Li films, showing a maximum efficiency of 11.6% for thermal neutron detection. The ^{6}Li film thickness required to match the performance of ^{10}B is approximately

5 times greater, and the optimum performance is achieved with a film thickness of approximately 95 μm. Due to thin-film stress-related problems, the authors have chosen to use ^{10}B for the present experiments.

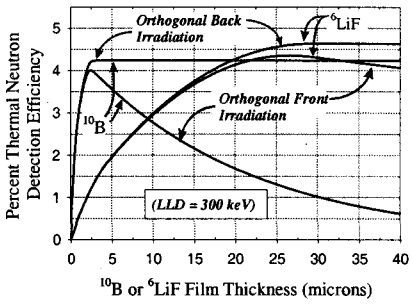

Fig. 1. Theoretical thermal neutron efficiency for front and back irradiated detectors coated with ^{10}B or ^{6}LiF.

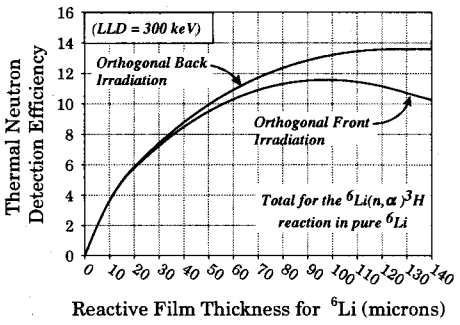

Fig. 2. Theoretical thermal neutron efficiency for front and back irradiated detectors coated with ^{6}Li

4. HDPE Coated Detectors

High-density polyethlyene (HDPE) coated detectors are sensitive to recoil protons produced from elastic scattering in the hydrogen. Although ^{10}B has a large thermal neutron cross section, it has a much lower neutron cross section for epithermal and fast neutrons. On the other hand, hydrogen-filled materials can be used to produce energetic protons through elastic scattering. The scattering cross section for hydrogen is larger than the absorption cross section for ^{10}B for neutron energies above 1 keV, but it is much lower than the absorption cross section for ^{10}B for neutron energies below 1 keV.

For fast neutrons (neutrons exceeding of 500 keV), a hydrogen-rich coating such as HDPE will produce relatively good detection efficiency.

The recoil proton energy is dependent on the initial neutron energy [17]. The fast neutron cross section for scattering is very low, therefore the addition of thin HDPE layers on the detector do not significantly degrade the neutron beam. The intrinsic efficiency was calculated as a function of neutron energy for different coating thicknesses, the results of which are discussed elsewhere [17]. It was found that maximum efficiency for 14 MeV neutrons was limited to HDPE films of 2200 ?m thickness, the maximum range of a 14 MeV proton in HDPE.

The expected detection responses from a variety of HDPE film thicknesses were analyzed, and it was observed that the spectral response of the detector can be tailored by varying the HDPE coating thickness [17]. For any given neutron energy, the detector efficiency is maximized for a coating thickness that matches the maximum range of a proton with the same energy. This would occur for a scattering event in which the proton was ejected at a zero degree angle or directly forward.

Directional dependence of the HDPE coated detectors is readily apparent from the kinematics of elastic scattering from hydrogen. Recoil protons do not scatter in the backward direction. Furthermore, the proton energy is a strong function of the scattering angle. A neutron transfers all of its energy to forward-scattered (0^{o}) protons and transfers none of its energy to 90^{o} scattered protons. No detectable response is observed if the detector is not facing the source [6], hence HDPE-coated detectors are directionally sensitive.

DETECTOR CONSTRUCTION

Two basic diode constructions were investigated, those being Schottky Barrier devices and high-purity p-i-n devices. Referring to Figure 3A, the Schottky barrier devices were fabricated from semi-insulating (SI) updoped GaAs wafers. SI GaAs wafers were lapped and polished to 200 microns thick and patterned for a variety of different contacts. The conductive low resistance back contacts (or "ohmic contacts) were composed of a layering of Ni, Au, and Ge, which were subsequently annealed at 400°C. The Schottky barriers were composed of 150 angstroms of Ti upon which an additional 450 angstroms of Au was deposited. Afterwards, layers of 98% purified ^{10}B ranging in thickness from 1000 angstroms up to 2 microns were evaporated upon the Schottky contacts. Simple designs take advantage of the truncated electric field effect present with bulk SI GaAs [18], thereby reducing the operating voltage required to only 10 - 20 volts. Single pad detectors were 5 mm^2 in area, and multi-detector devices consisted of two rows (dual in-line) of 0.5 mm × 1.0 mm ^{10}B-coated pixels.

Self-biased devices consisted of p-i-n diodes with construction similar to the profile shown in Figure 3B. The devices were fabricated from n-type GaAs wafers, upon which high-purity regions were grown using low-pressure metal-organic chemical vapor deposition [4]. The intrinsic regions, unintentionally doped as ν -type from background impurities, range in thickness from 1 micron up to 5 microns, which are sufficiently thick to absorb all or most of the energy from the $^{10}B(n,\alpha)^7Li$ reaction products. Grown upon the intrinsic regions were thin (200 angstroms) p-type regions that served as blocking (rectifying) contacts. The "built-in" potential [21] of the p-ν interface is sufficient to operate the device, hence the p-i-n structures require no bias voltage, a clear advantage for remotely operated neutron detectors.

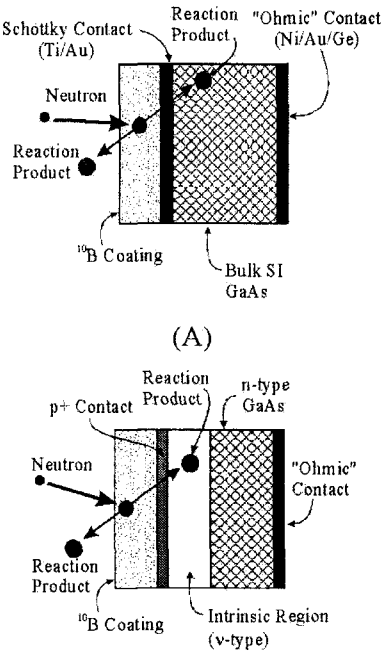

Fig. 3. The two basic device configurations investigated thus far are (A) SI bulk GaAs Schottky barrier structures and (B) high-purity p-i-n structures.

EXPERIMENTAL RESULTS

1. Neutron Measurements

The mounted GaAs devices were installed into aluminum testing boxes designed to reduce radiofrequency (RF) and photoelectric noise [4,5].

The box design allowed for repeatable indexing of the detectors in the center of the thermal neutron beam. A standard Ortec 142A preamplifier was connected to the SI bulk GaAs devices and the self-biased p-i-n GaAs devices. Spectra were recorded on an MCA. One-hour duration measurements were performed, and the dead time was adjusted and maintained at 2%.

Thermal neutron measurements were performed with a double diffracted beam emanating from a 2 MW materials test reactor. The beam port is not aligned with the reactor core, but instead faces into a heavy water (D_2O) tank. The beam is then diffracted off of two single crystal copper plates to further reduce background gamma ray contamination [3,5]. A fission chamber was used to calibrate

the neutron flux emerging from beam port, which gave a value of approximately $\Phi = 2.7 \times 10^4$ n/cm^2-s. Control rod movements contributed to some small change in the neutron flux value over the duration of the experiment, and adjacent beam port experiments also contributed to changes in neutron background. The changes in the neutron flux amounted to a few percent (2-3%) and the calibrated flux quoted represents only an average measurement.

Both sides of the detector were tested facing the neutron beam: the Schottky contact side was first tested followed by the ohmic contact side. Although the ohmic contact side did not have a ^{10}B coating on it, thermal neutrons pass through the GaAs detector and still become absorbed in the ^{10}B film. Figure 4 shows a typical spectrum from a ^{10}B-coated self-biased detector, in which the reaction product energies are clearly discernable. The peak resolution was observed to decrease with increasing film thickness (a result of charged particle self-absorption), yet the efficiency increases. Since the devices are operated as counters and not spectrometers, count rate is most important, hence thicker films are desirable. By summing the number of counts in the channels exceeding 300 keV, the efficiency was determined for several devices as a function of ^{10}B-film thickness for both obverse and reverse irradiations (see Figure 5). Also shown is the theoretical thermal neutron efficiency curve for an *LLD* setting of 300 keV, the curve having been calculated from equations 1-3. Figure 5 shows good agreement with the developed theory and the measurements.

Fast neutron measurements were performed using a MF Physics Model A-711 neutron generator which produces 14 MeV neutrons from D-T reactions. From over 200 hours of operation on the generator tube, the exact neutron output of the device is unknown, making it difficult to determine the fast neutron detection efficiency. The detectors were placed approximately 10 cm from the front of the neutron generator tube and all were operated at 120 volts bias. The measurement periods for each detector were 120 s.

Figure 6 shows a comparison between a bare detector, a detector coated with 125μm of HDPE, and a detector coated with 875μm of HDPE. As expected, the fast neutron detection efficiency is greater for the thicker HDPE film. The total count rate for a detector with 875μm of HDPE coating was 948 cps, while the total count rate above the "valley"(channel 65) was 504 cps. The total count rate for the detector with a 125μm HDPE coating was 744 cps, while the total count rate above the "valley"

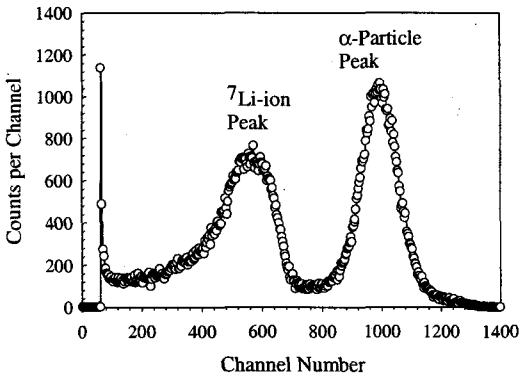

Fig. 4. Thermal neutron detection efficiency for both front and back irradiation as a function of ^{10}B-film thickness.

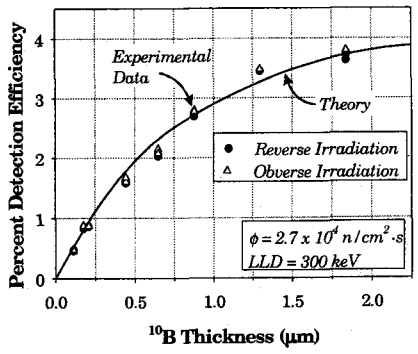

Fig. 5. Typical ^{10}B(n,α)^{7}Li product spectra from a self-biased p-i-n detector (^{10}B thickness = 5000 angstroms). The reaction product features are readily apparent [6].

was only 208 cps. Apparently, the counting efficiency does not scale linearly with HDPE thickness, a similar condition found with ^{10}B-coated devices for thermal neutrons. Further tests with Cd shielding were conducted to determine the effect of down-scattered neutrons, in which it was determined that the devices were detecting mostly fast neutrons with a minimal thermal component [6].

2. Radiation Hardness

Several detector variations were tested by irradiating the devices with a 20 kCi ^{60}Co gamma rays source and within the moderator pool of a 2 MW nuclear reactor. The experiments were conducted in such a way that the damage effects from gamma rays, neutrons, and charged particle reaction products were isolated [5]. The study clearly demonstrated that the GaAs devices were sufficiently resilient to gamma ray and neutron irradiation, however the charged particle reaction products from the $^{10}B(n,\alpha)^{7}Li$ reaction caused noticeable degradation at thermal neutron fluences of 1013 n/cm^2. Using 2% as the efficiency measured for the devices (5000 angstroms of ^{10}B), it is apparent that catastrophic damage occurs for a reaction product fluence of 2×10^{11}/cm^2. Figure 7 shows the relative measured thermal neutron count rate as a function of thermal neutron fluence, demonstrating the onset of failure at 10^{13} n /cm^2.

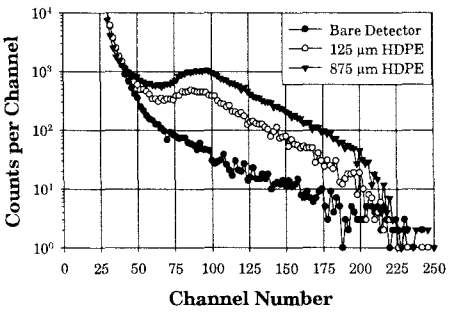

Fig. 6. Proton recoil spectra from 14 MeV neutrons taken with an HDPE-coated GaAs detector [6].

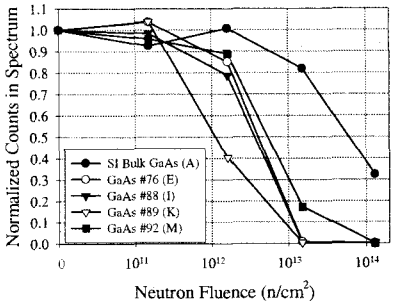

Fig. 7. Count rate degradation for various 10B-coated GaAs detectors as a function of thermal neutron fluence. Shown are results from a SI bulk GaAs device and several p-i-n devices [5].

3. Array Measurements

Dual in-line SI bulk GaAs arrays with 0.5 mm × 1 mm pixels were connected to a multi-preamplifier circuit allowing for real time readout of 16 pixels. The device was encased in an aluminum box to prevent interference from light and electromagnetic noise. The device was operated in neutron beam from a 2 MW material test reactor and step-scanned across several objects. Each step in the scan allowed for a 600-second count. The calibrated neutron flux was 2 × 10^6 n/cm^2-s along with a gamma ray background of 1 R/hr. The thin features of the detectors reduced interference from gamma ray background [6].

A variety of measurements were conducted to obtain contrast profiles for different materials. Figure 8 shows a count rate profile of an aluminum block filled with water columns, in which the aluminum block edges and the column location are easily distinguished. Step wedges of varying thickness were used to determine the overall contrast,

including steel, copper, aluminum, and polyethylene wedges. Figure 9 shows the contrast in neutron count rate for a steel step wedge, demonstrating that each step in the wedge is easily discerned. The polyethylene wedge was the most difficult to image due to high thermal neutron scattering. Still, the steps in the polyethylene wedge were discernable.

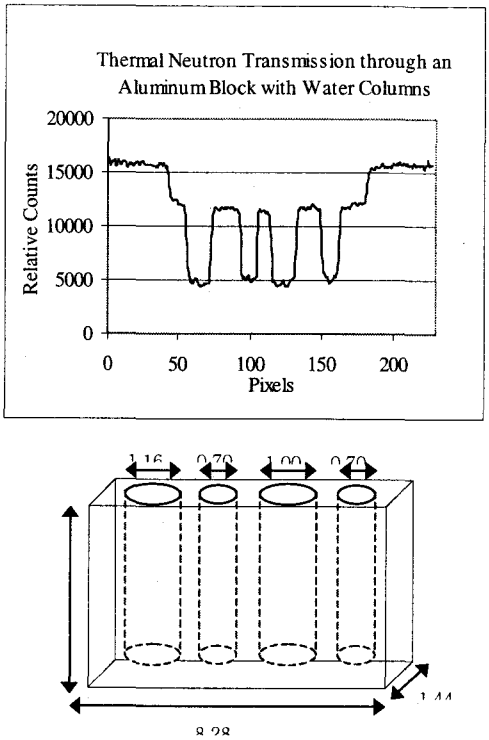

Fig. 8. Count rate profile taken with a dual in-line ^{10}B-coated pixel array of an aluminum block filled with different diameters of water columns (dimensions in cm).

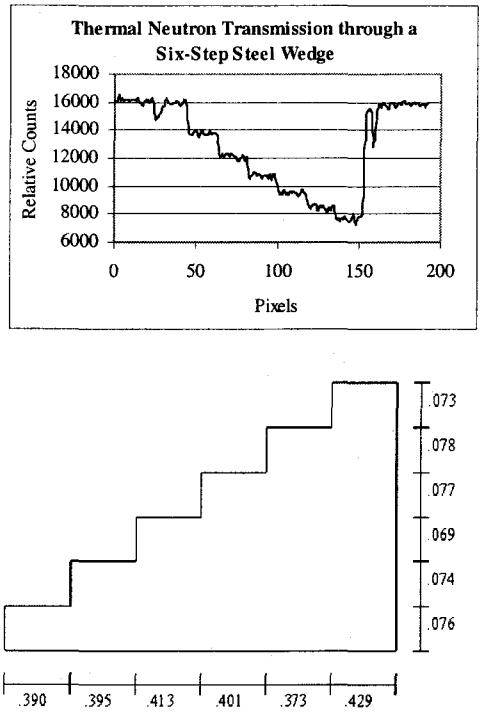

Fig. 9. Count rate profile taken with a dual in-line ^{10}B-coated pixel array of a steel step wedge (dimensions in inches).

FUTURE DEVELOPMENTS AND SUMMARY

^{10}B-coated GaAs devices have been demonstrated as viable compact thermal neutron detectors. They can be used under low power conditions and can withstand thermal neutron fluences up to 10^{13} n/cm^2 before noticeable degradation begins to occur. The devices are relatively inexpensive to produce and are reliable. Additionally, pixelated arrays can be developed and integrated onto GaAs wafers (or silicon) due to the maturity of the technology.

Future devices will incorporate the use of Li-based films to reduce gamma ray background effects. The films, either ^6LiF or pure ^6Li, will be tailored to optimize film thickness. Encapsulation techniques to prevent Li decomposition are being explored. Also, low gamma ray absorbing substrates will be investigated as alternatives to GaAs. At present, SiC is under investigation as a possible alternative substrate, mainly because of its low average atomic number, its thermal tolerance, and its radiation hardness.

REFERENCES

1. A.J. Peurrung, Nucl. Instr. and Meth., A443 (2000).
2. A. Rose, Nucl. Instr. and Meth., 52 (1967).
3. D.S. McGregor, J.T. Lindsay, C.C. Brannon, and R.W. Olsen, IEEE Trans. Nucl. Sci., NS-43 (1996).
4. D.S. McGregor, S.M. Vernon, H.K. Gersch, S.M. Markham, S.J. Wojtczuk, and D.K. Wehe, IEEE Trans. Nuclear Science, 47 (2000).
5. H.K. Gersch, D.S. McGregor, and P.A. Simpson, Conf. Record of the IEEE Nuclear Science Symposium, Lyon, France, Oct. 15-20, (2000).

6. D.S. McGregor, R.T. Klann, H.K. Gersch, and Y-H. Yang, Nucl. Instr. and Meth., A466 (2001).
7. I.C. Rickard, Nucl. Instr. and Meth., 113 (1973).
8. S.Pospisil, B. Sopko, E. Harrankova, Z. Janout, J. Konicek, I Macha, and J. Pavlu, Radiation Protection Dosimetry, 46 (1993).
9. J. Schelten, R. Reinartz, R. Engels, M. Balzhauser, J. Lauter, W Schafer, and K.D. Muller, Nucl. Instr. and Meth., A389 (1997).
10. B. Feigl and H. Rauch, Nucl. Instr. and Meth., 61 (1968).
11. R.L. Schulte, F. Swanson and M. Kesselman, Nucl. Instr. and Meth., A353 (1994).
12. A. Mireshghi, G. Cho, J.S. Drewery, W.S. Hong, T. Jing, H. Lee, S.N. Kaplan, and V. Perez-Mendez, IEEE Trans. Nucl. Sci., NS-41 (1994).
13. C. Petrillo, F.Sacchetti, O. Toket, and N.J. Rhodes, Nucl. Instr. and Meth., A 378 (1996).
14. F. Foulon, P. Bergonzo, A. Brambilla, C. Jany, B. Guizard, and R.D. Marshall, Proc. MRS, 487 (1998).
15. H. Gotoh and H. Yagi, Nucl. Instr. and Meth., 101 (1972).
16. F. Shirashi, Y. Takami, H. Husimi, S. Ohkawa, C. Kim, Y. Kim, K. Kikuchi, and T. Sakai, IEEE Trans. Nucl. Sci., NS-32 (1985).
17. R.T. Klann, C. L. Fink, D. S. McGregor, and H. K. Gersch, presented at the 15th Int. Conf. on Applications of Accelerators in Research and Industry, November,(2000).
18. D.S. McGregor and J.E. Kammeraad, Semiconductors and Semimetals, Vol. 43, Chap. 10 (Academic Press, San Diego, 1995).
19. V. McLane, C.L. Dunford, and P.F. Rose, Neutron Cross Sections, Vol. 2 (Academic Press, San Diego, 1988).
20. G.F. Knoll, Radiation Detection and Measurement, 3rd Ed.(Wiley, New York, 2000).
21. S.M. Sze, Physics of Semiconductor Devices, 2nd Ed. (Wiley, New York, 1981).